

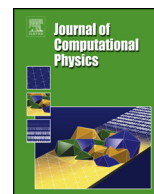


ELSEVIER

Contents lists available at ScienceDirect

Journal of Computational Physics

www.elsevier.com/locate/jcp



An efficient fully-discrete local discontinuous Galerkin method for the Cahn–Hilliard–Hele–Shaw system

Ruihan Guo, Yinhua Xia¹, Yan Xu^{*,2}

School of Mathematical Sciences, University of Science and Technology of China, Hefei, Anhui 230026, PR China

ARTICLE INFO

Article history:

Received 30 August 2013

Received in revised form 31 December 2013

Accepted 22 January 2014

Available online 27 January 2014

Keywords:

Cahn–Hilliard–Hele–Shaw system

Local discontinuous Galerkin method

Energy stability

Convex splitting

Multigrid

ABSTRACT

In this paper, we develop an efficient and energy stable fully-discrete local discontinuous Galerkin (LDG) method for the Cahn–Hilliard–Hele–Shaw (CHHS) system. The semi-discrete energy stability of the LDG method is proved firstly. Due to the strict time step restriction ($\Delta t = \mathcal{O}(\Delta x^4)$) of explicit time discretization methods for stability, we introduce a semi-implicit time integration scheme which is based on a convex splitting of the discrete Cahn–Hilliard energy. The unconditional energy stability has been proved for this fully-discrete LDG scheme. The fully-discrete equations at the implicit time level are nonlinear. Thus, the nonlinear Full Approximation Scheme (FAS) multigrid method has been applied to solve this system of algebraic equations, which has been shown the nearly optimal complexity numerically. Numerical results are also given to illustrate the accuracy and capability of the LDG method coupled with the multigrid solver.

© 2014 Elsevier Inc. All rights reserved.

1. Introduction

In this paper, we consider numerical methods in a bounded domain $\Omega \in \mathbb{R}^d$ ($d \leq 3$) for the Cahn–Hilliard–Hele–Shaw (CHHS) system:

$$\begin{aligned}\phi_t &= \Delta\mu - \nabla \cdot (\phi \mathbf{u}), \\ \mathbf{u} &= -\nabla p - \gamma \phi \nabla \mu, \\ \nabla \cdot \mathbf{u} &= 0,\end{aligned}\tag{1.1}$$

where $\gamma > 0$, \mathbf{u} is the advective velocity, p is the pressure and μ is the chemical potential

$$\mu = \phi^3 - \phi - \varepsilon^2 \Delta \phi.$$

Numerical methods to simulate the solution of the CHHS system are few. Wise [22] introduced an unconditionally stable finite difference method for the CHHS system. Feng and Wise [13] presented finite element analysis for a system of partial differential equations (PDEs) consisting of the Darcy equation and the Cahn–Hilliard (CH) equation. Collins [11] presented an unconditionally energy stable and uniquely solvable finite difference scheme for the Cahn–Hilliard–Brinkman system, which was comprised of a Cahn–Hilliard-type diffusion equation and a generalized Brinkman equation modeling fluid flow. When

* Corresponding author.

E-mail addresses: guoguo88@mail.ustc.edu.cn (R. Guo), yhxia@ustc.edu.cn (Y. Xia), yxu@ustc.edu.cn (Y. Xu).

¹ Research supported by NSFC grant No. 11101400, No. 11371342, Doctoral Fund of Ministry of Education of China No. 20113402120015 and SRF for ROCS SEM.

² Research supported by NSFC grant No. 11371342, No. 11031007, FANEDD No. 200916, Fok Ying Tung Education Foundation No. 131003.

$\gamma = 0$, the CHHS system is reduced to the CH equation [5]. Many numerical methods have been developed to treat the CH equation, using finite elements [1–3], multigrid methods [16–18] and finite difference methods [12,14,20]. Xia et al. [23] developed a local discontinuous Galerkin (LDG) method for the CH equation and proved the energy stability. Guo and Xu studied the multigrid solver coupled with the LDG method for the CH equation in [15].

Solutions of the CHHS system generally have boundary layers spread throughout the domain, so spatial resolution is extremely important in the choice of numerical schemes. In this paper, we introduce an LDG method for the CHHS system, which is high order accurate, nonlinear stable and flexible for arbitrary h and p adaptivity. The semi-discrete energy stability of the LDG method is also proved.

For the fourth order nonlinear CHHS system, explicit time discretization methods will require severe time step restriction ($\Delta t = \mathcal{O}(\Delta x^4)$), so we explore implicit methods. Following the method introduced by Wise [22], we develop a semi-implicit time integration scheme based on a convex splitting of the discrete Cahn–Hilliard energy. We also prove the unconditional discrete energy stability of the fully-discrete LDG scheme, i.e. the scheme is stable regardless of time step size. Being implicit in time, the equations at the implicit time level are nonlinear. The efficiency of the implicit method highly depends on the efficiency of the nonlinear solver. The nonlinear Gauss–Seidel method and the Newton method can be used to solve the nonlinear equations, but they suffer from slow convergence rates for large system. In this paper, we apply the nonlinear Full Approximation Scheme (FAS) multigrid method to solve the nonlinear equations arising by the semi-implicit scheme. In particular, we numerically show that the multigrid solver has nearly optimal complexity.

The discontinuous Galerkin (DG) method we discuss in this paper is a class of finite element methods, using discontinuous, piecewise polynomials as the solution and test space. Reed and Hill [19] first introduced the DG method in 1973, in the framework of neutron linear transport. Cockburn et al. [6–9] applied the DG method for solving nonlinear hyperbolic conservation laws.

For PDEs containing higher order spatial derivatives, it is difficult to apply the DG method directly, so the LDG method was introduced. The idea of the LDG method is to rewrite the equations with higher order derivatives as a first order system, then apply the DG method to the system. The first LDG method was constructed by Cockburn and Shu in [10] for solving nonlinear convection diffusion equations containing second order spatial derivatives. Their work was motivated by the successful numerical experiments of Bassi and Rebay [4] for the compressible Navier–Stokes equations. Yan and Shu developed an LDG method for a general KdV type equation (containing third order spatial derivatives) in [26], and they generalized the LDG method to PDEs with fourth and fifth order spatial derivatives in [27]. Xia et al. [23,24] developed the LDG method to solve the Cahn–Hilliard type equations and the Allen–Cahn/Cahn–Hilliard system. For a detailed description about the LDG methods for high-order time-dependent PDEs, we refer the readers to [25]. A common feature of these LDG methods is that stability can be proved for quite general nonlinear cases. DG and LDG methods also have several attractive properties, such as their flexibility for general geometry, unstructured meshes, arbitrary hp adaptivity and their excellent parallel efficiency.

This paper is organized as follows. In Section 2, we present the LDG method for the CHHS system and prove the energy stability. In Section 3, we introduce a semi-implicit time integration method and prove an unconditional discrete energy stability for the fully-discrete scheme. Section 4 contains numerical results for the nonlinear CHHS system. The numerical results demonstrate the accuracy and capability of the LDG method and the multigrid solver. Finally, we give concluding remarks in Section 5. In Appendix A, we give a detailed description of the nonlinear FAS multigrid method.

2. The LDG method for the Cahn–Hilliard–Hele–Shaw system

2.1. Energy stability of the Cahn–Hilliard–Hele–Shaw system

The CHHS system was developed to model spinodal decomposition of a binary fluid in a Hele–Shaw cell, tumor growth and cell sorting, and two phase flows in porous media. The CHHS equation (1.1) can be written into the following form

$$\phi_t = \Delta\mu + \nabla \cdot (\phi(\nabla p + \gamma\phi\nabla\mu)), \quad (2.2a)$$

$$\mu = \phi^3 - \phi - \varepsilon^2\Delta\phi, \quad (2.2b)$$

and p will be obtained from the following Laplacian equation

$$-\Delta p = \gamma\nabla \cdot (\phi\nabla\mu). \quad (2.3)$$

In the CHHS system, ϕ is the concentration field, γ and ε are constants. The phase equilibria are represented by the pure fluids $\phi = \pm 1$. We assume no flux boundary conditions, namely $\mathbf{u} \cdot \mathbf{n} = 0$ and $\partial_n\mu = 0$ on $\partial\Omega$. We can clearly see that the boundary condition for the velocity \mathbf{u} is equivalent to $\partial_n p = 0$ on $\partial\Omega$. Thus, in this paper, the boundary conditions are assumed as

$$\partial_n\phi = \partial_n\mu = \partial_n p = 0, \quad \text{on } \partial\Omega. \quad (2.4)$$

The system (2.2)–(2.3) is mass conservative and energy dissipative, i.e.

$$\frac{d}{dt} E = - \int_{\Omega} \left(|\nabla \mu|^2 + \frac{1}{\gamma} |\mathbf{u}|^2 \right) d\mathbf{x} \leq 0, \tag{2.5}$$

where

$$E = \int_{\Omega} \left(\frac{1}{4} \phi^4 - \frac{1}{2} \phi^2 + \frac{\varepsilon^2}{2} |\nabla \phi|^2 \right) d\mathbf{x}. \tag{2.6}$$

2.2. The LDG method for the Cahn–Hilliard–Hele–Shaw system

In this subsection, we develop the LDG method for the CHHS system in $\Omega \in \mathbb{R}^d$ with $d \leq 3$. Although we do not perform numerical experiments in three dimensions in this paper, the LDG method and the energy stability results of this paper are valid for all $d \leq 3$.

2.2.1. Notations

Let \mathcal{T}_h denote a tessellation of Ω with shape-regular elements K . Let Γ denote the union of the boundary faces of elements $K \in \mathcal{T}_h$, i.e. $\Gamma = \bigcup_{K \in \mathcal{T}_h} \partial K$, and $\Gamma_0 = \Gamma \setminus \partial \Omega$. In order to describe the flux functions, we need to introduce some notations. Let e be a face shared by the “left” and “right” elements K_L and K_R . For our purpose “left” and “right” can be uniquely defined for each face according to any fixed rule, see, e.g. [25,26] for more details of such a definition. Define the normal vectors \mathbf{v}_L and \mathbf{v}_R on e pointing exterior to K_L and K_R , respectively. If ψ is a function on K_L and K_R , but possibly discontinuous across e , let ψ_L denote $(\psi|_{K_L})|_e$ and ψ_R denote $(\psi|_{K_R})|_e$, the left and right trace, respectively.

Let $\mathcal{P}^k(K)$ be the space of polynomials of degree at most $k \geq 0$ on $K \in \mathcal{T}_h$. The finite element spaces are denoted by

$$V_h = \{ \varphi : \varphi|_K \in \mathcal{P}^k(K), \forall K \in \mathcal{T}_h \},$$

$$\Sigma_h^d = \{ \Phi = (\phi_1, \dots, \phi_d)^T : \phi_l|_K \in \mathcal{P}^k(K), l = 1, \dots, d, \forall K \in \mathcal{T}_h \}.$$

Note that functions in V_h, Σ_h^d are allowed to be completely discontinuous across element interfaces.

2.2.2. The LDG method

To construct the LDG method, firstly we rewrite the Cahn–Hilliard–Hele–Shaw system (2.2)–(2.3) as a system containing only first order derivatives:

$$\phi_t = \nabla \cdot \mathbf{w} + \nabla \cdot \mathbf{s}, \tag{2.7a}$$

$$\mathbf{w} = \nabla \mu, \tag{2.7b}$$

$$\mu = \phi^3 - \phi - \varepsilon^2 \nabla \cdot \mathbf{v}, \tag{2.7c}$$

$$\mathbf{v} = \nabla \phi, \tag{2.7d}$$

$$\mathbf{s} = \phi(\mathbf{q} + \gamma \phi \mathbf{w}) \tag{2.7e}$$

and

$$-\nabla \cdot \mathbf{q} = \gamma \nabla \cdot \mathbf{r}, \tag{2.8a}$$

$$\mathbf{q} = \nabla p, \tag{2.8b}$$

$$\mathbf{r} = \phi \mathbf{w}. \tag{2.8c}$$

To simplify the notation, we still use $\phi, \mathbf{w}, \mu, \mathbf{v}, \mathbf{s}, \mathbf{q}, \mathbf{r}$ and p to denote the numerical solution. The LDG scheme to solve the Cahn–Hilliard–Hele–Shaw system (2.7) and (2.8) is as follows: Find $\phi, \mu, p \in V_h$ and $\mathbf{w}, \mathbf{v}, \mathbf{s}, \mathbf{q}, \mathbf{r} \in \Sigma_h^d$, such that, for all test functions $\varphi, \psi, \xi \in V_h$ and $\Phi, \Psi, \zeta, \eta, \rho \in \Sigma_h^d$

$$\int_K \phi_t \varphi dK = - \int_K (\mathbf{w} + \mathbf{s}) \cdot \nabla \varphi dK + \int_{\partial K} (\widehat{\mathbf{w}} \cdot \mathbf{v} + \widehat{\mathbf{s}} \cdot \mathbf{v}) \varphi ds, \tag{2.9a}$$

$$\int_K \mathbf{w} \cdot \Phi dK = - \int_K \mu \nabla \cdot \Phi dK + \int_{\partial K} \widehat{\mu} \Phi \cdot \mathbf{v} ds, \tag{2.9b}$$

$$\int_K \mu \psi dK = \int_K (\phi^3 - \phi) \psi dK + \int_K \varepsilon^2 \mathbf{v} \cdot \nabla \psi dK - \int_{\partial K} \varepsilon^2 \widehat{\mathbf{v}} \cdot \mathbf{v} \psi ds, \tag{2.9c}$$

$$\int_K \mathbf{v} \cdot \Psi \, dK = - \int_K \phi \nabla \cdot \Psi \, dK + \int_{\partial K} \widehat{\phi} \Psi \cdot \mathbf{v} \, ds, \quad (2.9d)$$

$$\int_K \mathbf{s} \cdot \zeta \, dK = \int_K \phi (\mathbf{q} + \gamma \phi \mathbf{w}) \cdot \zeta \, dK \quad (2.9e)$$

and

$$\int_K \mathbf{q} \cdot \nabla \xi \, dK - \int_{\partial K} \widehat{\mathbf{q}} \cdot \mathbf{v} \xi \, ds = -\gamma \int_K \mathbf{r} \cdot \nabla \xi \, dK + \gamma \int_{\partial K} \widehat{\mathbf{r}} \cdot \mathbf{v} \xi \, ds, \quad (2.10a)$$

$$\int_K \mathbf{q} \cdot \boldsymbol{\eta} \, dK = - \int_K p \nabla \cdot \boldsymbol{\eta} \, dK + \int_{\partial K} \widehat{p} \boldsymbol{\eta} \cdot \mathbf{v} \, ds, \quad (2.10b)$$

$$\int_K \mathbf{r} \cdot \boldsymbol{\rho} \, dK = \int_K \phi \mathbf{w} \cdot \boldsymbol{\rho} \, dK. \quad (2.10c)$$

The “hat” terms in (2.9)–(2.10) in the cell boundary terms from integration by parts are the so-called “numerical fluxes”, which are functions defined on the edges and should be designed based on different guiding principles for different PDEs to ensure stability and local solvability of the intermediate variables. It turns out that we can take the simple choices such as

$$\widehat{\mathbf{w}}|_e = \mathbf{w}_L, \quad \widehat{\mathbf{s}}|_e = \mathbf{s}_L, \quad \widehat{\mu}|_e = \mu_R, \quad \widehat{\phi}|_e = \phi_L, \quad \widehat{\mathbf{v}}|_e = \mathbf{v}_R, \quad (2.11)$$

and

$$\widehat{\mathbf{r}}|_e = \mathbf{r}_L, \quad \widehat{\mathbf{q}}|_e = \mathbf{q}_L, \quad \widehat{p}|_e = p_R. \quad (2.12)$$

By the boundary conditions (2.4), we take

$$\widehat{\mathbf{w}} = \mathbf{0}, \quad \widehat{\mathbf{s}} = \mathbf{0}, \quad \widehat{\mu} = \mu^{\text{in}}, \quad \widehat{\phi} = \phi^{\text{in}}, \quad \widehat{\mathbf{v}} = \mathbf{0}, \quad (2.13)$$

and

$$\widehat{\mathbf{r}} = \mathbf{0}, \quad \widehat{\mathbf{q}} = \mathbf{0}, \quad \widehat{p} = p^{\text{in}}, \quad (2.14)$$

at the domain boundary, where ϕ^{in} means the value taken from the inside of the boundary element. We remark that the choice for the fluxes (2.11)–(2.12) is not unique. Considering the compactness of the stencil and the optimal accuracy, the crucial part is taking $\widehat{\mathbf{w}}$, $\widehat{\mathbf{s}}$ and $\widehat{\mu}$ from opposite sides, $\widehat{\mathbf{v}}$ and $\widehat{\phi}$ from opposite sides, $\widehat{\mathbf{q}}$, $\widehat{\mathbf{r}}$ and \widehat{p} from opposite sides.

2.2.3. Energy dissipative

It is easy to show that the LDG scheme is mass conservative. And also we can prove the semi-discrete scheme is energy stable in the following.

Proposition 2.1 (Energy dissipative). *The solution to the LDG scheme (2.9)–(2.10) and the flux (2.11)–(2.12) with the boundary conditions (2.13)–(2.14) satisfies energy dissipative*

$$\frac{d}{dt} E = - \int_{\Omega} \left(|\mathbf{w}|^2 + \frac{1}{\gamma} |\mathbf{q} + \gamma \phi \mathbf{w}|^2 \right) d\mathbf{x} \leq 0, \quad (2.15)$$

where

$$E = \int_{\Omega} \left(\frac{1}{4} \phi^4 - \frac{1}{2} \phi^2 + \frac{\varepsilon^2}{2} |\mathbf{v}|^2 \right) d\mathbf{x}. \quad (2.16)$$

Proof. Firstly, we take the time derivative of Eq. (2.9d) and choose the test function $\Psi = \varepsilon^2 \mathbf{v}$ to obtain

$$\varepsilon^2 \int_K \mathbf{v}_t \cdot \mathbf{v} \, dK = -\varepsilon^2 \int_K \phi_t \nabla \cdot \mathbf{v} \, dK + \varepsilon^2 \int_{\partial K} \widehat{\phi}_t \mathbf{v} \cdot \mathbf{v} \, ds. \quad (2.17)$$

For other equations in (2.9)–(2.10), we choose the test functions

$$\varphi = \mu, \quad \Phi = \mathbf{w} + \mathbf{s}, \quad \psi = -\phi_t, \quad \zeta = -\mathbf{w}, \quad \xi = \frac{1}{\gamma} p, \quad \eta = \frac{1}{\gamma} \mathbf{q} + \mathbf{r}, \quad \rho = -\mathbf{q},$$

respectively to get

$$\begin{aligned} \int_K \phi_t \mu \, dK &= - \int_K (\mathbf{w} + \mathbf{s}) \cdot \nabla \mu \, dK + \int_{\partial K} (\widehat{\mathbf{w}} \cdot \mathbf{v} + \widehat{\mathbf{s}} \cdot \mathbf{v}) \mu \, ds, \\ \int_K \mathbf{w} \cdot (\mathbf{w} + \mathbf{s}) \, dK &= - \int_K \mu \nabla \cdot (\mathbf{w} + \mathbf{s}) \, dK + \int_{\partial K} \widehat{\mu} (\mathbf{w} + \mathbf{s}) \cdot \mathbf{v} \, ds, \\ - \int_K \mu \phi_t \, dK &= - \int_K (\phi^3 - \phi) \phi_t \, dK - \int_K \varepsilon^2 \mathbf{v} \cdot \nabla \phi_t \, dK + \int_{\partial K} \varepsilon^2 \widehat{\mathbf{v}} \cdot \mathbf{v} \phi_t \, ds, \\ - \int_K \mathbf{s} \cdot \mathbf{w} \, dK &= - \int_K \phi (\mathbf{q} + \gamma \phi \mathbf{w}) \cdot \mathbf{w} \, dK, \\ \frac{1}{\gamma} \int_K \mathbf{q} \cdot \nabla p \, dK - \frac{1}{\gamma} \int_{\partial K} p \widehat{\mathbf{q}} \cdot \mathbf{v} \, ds &= - \int_K \mathbf{r} \cdot \nabla p \, dK + \int_{\partial K} p \widehat{\mathbf{r}} \cdot \mathbf{v} \, ds, \\ \int_K \mathbf{q} \cdot \left(\frac{1}{\gamma} \mathbf{q} + \mathbf{r} \right) \, dK &= - \int_K p \nabla \cdot \left(\frac{1}{\gamma} \mathbf{q} + \mathbf{r} \right) \, dK + \int_{\partial K} \widehat{p} \left(\frac{1}{\gamma} \mathbf{q} + \mathbf{r} \right) \cdot \mathbf{v} \, ds, \\ - \int_K \mathbf{r} \cdot \mathbf{q} \, dK &= - \int_K \phi \mathbf{w} \cdot \mathbf{q} \, dK. \end{aligned}$$

Combining the above equations with (2.17), implies

$$\begin{aligned} \frac{d}{dt} \int_K \left(\frac{1}{4} \phi^4 - \frac{1}{2} \phi^2 + \frac{\varepsilon^2}{2} |\mathbf{v}|^2 \right) \, dK + \int_K \left(|\mathbf{w}|^2 + \frac{1}{\gamma} |\mathbf{q} + \gamma \phi \mathbf{w}|^2 \right) \, dK \\ = - \int_K \nabla \cdot (\mu (\mathbf{w} + \mathbf{s})) \, dK + \int_{\partial K} ((\widehat{\mathbf{w}} \cdot \mathbf{v} + \widehat{\mathbf{s}} \cdot \mathbf{v}) \mu + \widehat{\mu} (\mathbf{w} + \mathbf{s}) \cdot \mathbf{v}) \, ds \\ - \int_K \varepsilon^2 \nabla \cdot (\phi_t \mathbf{v}) \, dK + \varepsilon^2 \int_{\partial K} (\widehat{\phi}_t \mathbf{v} \cdot \mathbf{v} + \widehat{\mathbf{v}} \cdot \mathbf{v} \phi_t) \, ds \\ - \int_K \nabla \cdot \left(p \left(\frac{1}{\gamma} \mathbf{q} + \mathbf{r} \right) \right) \, dK + \int_{\partial K} \left(\widehat{p} \left(\frac{1}{\gamma} \mathbf{q} + \mathbf{r} \right) \cdot \mathbf{v} + p \left(\frac{1}{\gamma} \widehat{\mathbf{q}} + \widehat{\mathbf{r}} \right) \cdot \mathbf{v} \right) \, ds. \end{aligned} \tag{2.18}$$

Finally, summing up Eq. (2.18) over K and noticing the fluxes in (2.11)–(2.12) are from the opposite sides of ∂K as well as the boundary conditions (2.13)–(2.14), we have

$$\frac{d}{dt} \int_{\Omega} \left(\frac{1}{4} \phi^4 - \frac{1}{2} \phi^2 + \frac{\varepsilon^2}{2} |\mathbf{v}|^2 \right) \, d\mathbf{x} + \int_{\Omega} \left(|\mathbf{w}|^2 + \frac{1}{\gamma} |\mathbf{q} + \gamma \phi \mathbf{w}|^2 \right) \, d\mathbf{x} = 0,$$

which implies the result (2.15). \square

3. Time discretization

The LDG spatial discretization for the CHHS typically results in an ordinary differential equation (ODE). The CHHS system is a fourth order nonlinear partial differential equation and explicit time marching methods usually require severe time step ($\Delta t = \mathcal{O}(\Delta x^4)$) restriction for stability. Thus, we will explore an implicit time marching method to relax this constraint of the time step.

3.1. Fully-discrete LDG scheme

Wise [22] introduced an unconditionally stable finite difference scheme for the CHHS system based on a convex splitting of the discrete CH energy. Based on the work in [22], we apply the convex splitting method to the CHHS system coupled

with the LDG spatial discretization, and obtain an unconditionally stable LDG scheme. The fully-discrete convex splitting LDG scheme is

$$\frac{\phi^{n+1} - \phi^n}{\Delta t} = \Delta \mu^{n+1} + \nabla \cdot (\phi^n (\nabla p^{n+1} + \gamma \phi^n \nabla \mu^{n+1})), \quad (3.19a)$$

$$\mu^{n+1} = (\phi^{n+1})^3 - \phi^n - \varepsilon^2 \Delta \phi^{n+1}, \quad (3.19b)$$

$$-\Delta p^{n+1} = \gamma \nabla \cdot (\phi^n \nabla \mu^{n+1}). \quad (3.19c)$$

The LDG scheme for the fully-discrete scheme becomes: Find $\phi^{n+1}, \mu^{n+1}, p^{n+1} \in V_h$ and $\mathbf{w}^{n+1}, \mathbf{v}^{n+1}, \mathbf{s}^{n+1}, \mathbf{q}^{n+1}, \mathbf{r}^{n+1} \in \Sigma_h^d$, such that, for all test functions $\varphi, \psi, \xi \in V_h$ and $\Phi, \Psi, \zeta, \eta, \rho \in \Sigma_h^d$

$$\int_K \frac{\phi^{n+1} - \phi^n}{\Delta t} \varphi dK = - \int_K (\mathbf{w}^{n+1} + \mathbf{s}^{n+1}) \cdot \nabla \varphi dK + \int_{\partial K} (\widehat{\mathbf{w}^{n+1}} \cdot \mathbf{v} + \widehat{\mathbf{s}^{n+1}} \cdot \mathbf{v}) \varphi ds, \quad (3.20a)$$

$$\int_K \mathbf{w}^{n+1} \cdot \Phi dK = - \int_K \mu^{n+1} \nabla \cdot \Phi dK + \int_{\partial K} \widehat{\mu^{n+1}} \Phi \cdot \mathbf{v} ds, \quad (3.20b)$$

$$\int_K \mu^{n+1} \psi dK = \int_K ((\phi^{n+1})^3 - \phi^n) \psi dK + \int_K \varepsilon^2 \mathbf{v}^{n+1} \cdot \nabla \psi dK - \int_{\partial K} \varepsilon^2 \widehat{\mathbf{v}^{n+1}} \cdot \mathbf{v} \psi ds, \quad (3.20c)$$

$$\int_K \mathbf{v}^{n+1} \cdot \Psi dK = - \int_K \phi^{n+1} \nabla \cdot \Psi dK + \int_{\partial K} \widehat{\phi^{n+1}} \Psi \cdot \mathbf{v} ds, \quad (3.20d)$$

$$\int_K \mathbf{s}^{n+1} \cdot \zeta dK = \int_K \phi^n (\mathbf{q}^{n+1} + \gamma \phi^n \mathbf{w}^{n+1}) \cdot \zeta dK \quad (3.20e)$$

and

$$\int_K \mathbf{q}^{n+1} \cdot \nabla \xi dK - \int_{\partial K} \widehat{\mathbf{q}^{n+1}} \cdot \mathbf{v} \xi ds = -\gamma \int_K \mathbf{r}^{n+1} \cdot \nabla \xi dK + \gamma \int_{\partial K} \widehat{\mathbf{r}^{n+1}} \cdot \mathbf{v} \xi ds, \quad (3.21a)$$

$$\int_K \mathbf{q}^{n+1} \cdot \eta dK = - \int_K p^{n+1} \nabla \cdot \eta dK + \int_{\partial K} \widehat{p^{n+1}} \eta \cdot \mathbf{v} ds, \quad (3.21b)$$

$$\int_K \mathbf{r}^{n+1} \cdot \rho dK = \int_K \phi^n \mathbf{w}^{n+1} \cdot \rho dK. \quad (3.21c)$$

The numerical fluxes are

$$\widehat{\mathbf{w}^{n+1}}|_e = \mathbf{w}_L^{n+1}, \quad \widehat{\mathbf{s}^{n+1}}|_e = \mathbf{s}_L^{n+1}, \quad \widehat{\mu^{n+1}}|_e = \mu_R^{n+1}, \quad \widehat{\phi^{n+1}}|_e = \phi_L^{n+1}, \quad \widehat{\mathbf{v}^{n+1}}|_e = \mathbf{v}_R^{n+1}, \quad (3.22)$$

and

$$\widehat{\mathbf{r}^{n+1}}|_e = \mathbf{r}_L^{n+1}, \quad \widehat{\mathbf{q}^{n+1}}|_e = \mathbf{q}_L^{n+1}, \quad \widehat{p^{n+1}}|_e = p_R^{n+1}. \quad (3.23)$$

At the domain boundary, we take

$$\widehat{\mathbf{w}^{n+1}} = \mathbf{0}, \quad \widehat{\mathbf{s}^{n+1}} = \mathbf{0}, \quad \widehat{\mu^{n+1}} = (\mu^{n+1})^{\text{in}}, \quad \widehat{\phi^{n+1}} = (\phi^{n+1})^{\text{in}}, \quad \widehat{\mathbf{v}^{n+1}} = \mathbf{0}, \quad (3.24)$$

and

$$\widehat{\mathbf{r}^{n+1}} = \mathbf{0}, \quad \widehat{\mathbf{q}^{n+1}} = \mathbf{0}, \quad \widehat{p^{n+1}} = (p^{n+1})^{\text{in}}. \quad (3.25)$$

3.2. Discrete energy dissipative

In this subsection, we will prove the unconditional discrete energy stability for the fully-discrete LDG scheme (3.19). To simplify the notation, we use the following notations for discretization of time variable,

$$\delta_t \phi^{n+1} = \frac{\phi^{n+1} - \phi^n}{\Delta t},$$

$$\delta_t \mathbf{v}^{n+1} = \frac{\mathbf{v}^{n+1} - \mathbf{v}^n}{\Delta t}.$$

Proposition 3.1 (Discrete energy dissipative). *The solution to the LDG scheme (3.20)–(3.21) and the flux (3.22)–(3.23) with the boundary conditions (3.24)–(3.25) satisfies energy dissipative*

$$\int_{\Omega} \left(\frac{1}{4}(\phi^{n+1})^4 - \frac{1}{2}(\phi^{n+1})^2 + \frac{\varepsilon^2}{2}|\mathbf{v}^{n+1}|^2 \right) d\mathbf{x} \leq \int_{\Omega} \left(\frac{1}{4}(\phi^n)^4 - \frac{1}{2}(\phi^n)^2 + \frac{\varepsilon^2}{2}|\mathbf{v}^n|^2 \right) d\mathbf{x}.$$

Proof. We take the test functions in (3.20) as

$$\varphi = \mu^{n+1}, \quad \Phi = \mathbf{w}^{n+1} + \mathbf{s}^{n+1}, \quad \psi = -\delta_t \phi^{n+1}, \quad \Psi = \varepsilon^2 \delta_t \mathbf{v}^{n+1}, \quad \zeta = -\mathbf{w}^{n+1}.$$

For other equations in (3.21), we choose the test functions

$$\xi = \frac{1}{\gamma} p^{n+1}, \quad \eta = \frac{1}{\gamma} \mathbf{q}^{n+1} + \mathbf{r}^{n+1}, \quad \rho = -\mathbf{q}^{n+1}$$

to obtain

$$\begin{aligned} \int_K \delta_t \phi^{n+1} \mu^{n+1} dK &= - \int_K (\mathbf{w}^{n+1} + \mathbf{s}^{n+1}) \cdot \nabla \mu^{n+1} dK + \int_{\partial K} (\widehat{\mathbf{w}^{n+1}} \cdot \mathbf{v} + \widehat{\mathbf{s}^{n+1}} \cdot \mathbf{v}) \mu^{n+1} ds, \\ \int_K \mathbf{w}^{n+1} \cdot (\mathbf{w}^{n+1} + \mathbf{s}^{n+1}) dK &= - \int_K \mu^{n+1} \nabla \cdot (\mathbf{w}^{n+1} + \mathbf{s}^{n+1}) dK + \int_{\partial K} \widehat{\mu}^{n+1} (\mathbf{w}^{n+1} + \mathbf{s}^{n+1}) \cdot \mathbf{v} ds, \\ - \int_K \mu^{n+1} \delta_t \phi^{n+1} dK &= - \int_K ((\phi^{n+1})^3 - \phi^n) \delta_t \phi^{n+1} dK - \int_K \varepsilon^2 \mathbf{v}^{n+1} \cdot \nabla \delta_t \phi^{n+1} dK + \int_{\partial K} \varepsilon^2 \widehat{\mathbf{v}^{n+1}} \cdot \mathbf{v} \delta_t \phi^{n+1} ds, \\ \varepsilon^2 \int_K \mathbf{v}^{n+1} \cdot \delta_t \mathbf{v}^{n+1} dK &= -\varepsilon^2 \int_K \phi^{n+1} \nabla \cdot \delta_t \mathbf{v}^{n+1} dK + \varepsilon^2 \int_{\partial K} \widehat{\phi}^{n+1} \delta_t \mathbf{v}^{n+1} \cdot \mathbf{v} ds, \\ - \int_K \mathbf{s}^{n+1} \cdot \mathbf{w}^{n+1} dK &= - \int_K \phi^n (\mathbf{q}^{n+1} + \gamma \phi^n \mathbf{w}^{n+1}) \cdot \mathbf{w}^{n+1} dK, \end{aligned}$$

and

$$\begin{aligned} \frac{1}{\gamma} \int_K \mathbf{q}^{n+1} \cdot \nabla p^{n+1} dK - \frac{1}{\gamma} \int_{\partial K} \widehat{\mathbf{q}^{n+1}} \cdot \mathbf{v} p^{n+1} ds &= - \int_K \mathbf{r}^{n+1} \cdot \nabla p^{n+1} dK + \int_{\partial K} \widehat{\mathbf{r}^{n+1}} \cdot \mathbf{v} p^{n+1} ds, \\ \int_K \mathbf{q}^{n+1} \cdot \left(\frac{1}{\gamma} \mathbf{q}^{n+1} + \mathbf{r}^{n+1} \right) dK &= - \int_K p^{n+1} \nabla \cdot \left(\frac{1}{\gamma} \mathbf{q}^{n+1} + \mathbf{r}^{n+1} \right) dK + \int_{\partial K} \widehat{p}^{n+1} \left(\frac{1}{\gamma} \mathbf{q}^{n+1} + \mathbf{r}^{n+1} \right) \cdot \mathbf{v} ds, \\ - \int_K \mathbf{r}^{n+1} \cdot \mathbf{q}^{n+1} dK &= - \int_K \phi^n \mathbf{w}^{n+1} \cdot \mathbf{q}^{n+1} dK. \end{aligned}$$

Combining the above equations, we get

$$\begin{aligned} \varepsilon^2 \int_K \mathbf{v}^{n+1} \cdot \delta_t \mathbf{v}^{n+1} dK + \int_K ((\phi^{n+1})^3 - \phi^n) \delta_t \phi^{n+1} dK + \int_K \left(|\mathbf{w}^{n+1}|^2 + \frac{1}{\gamma} |\mathbf{q}^{n+1} + \gamma \phi^n \mathbf{w}^{n+1}|^2 \right) dK \\ = - \int_K \nabla \cdot (\mu^{n+1} (\mathbf{w}^{n+1} + \mathbf{s}^{n+1})) dK + \int_{\partial K} ((\widehat{\mathbf{w}^{n+1}} \cdot \mathbf{v} + \widehat{\mathbf{s}^{n+1}} \cdot \mathbf{v}) \mu^{n+1} + \widehat{\mu}^{n+1} (\mathbf{w}^{n+1} + \mathbf{s}^{n+1}) \cdot \mathbf{v}) ds \\ - \int_K \nabla \cdot \left(p^{n+1} \left(\frac{1}{\gamma} \mathbf{q}^{n+1} + \mathbf{r}^{n+1} \right) \right) dK + \int_{\partial K} \left(\widehat{p}^{n+1} \left(\frac{1}{\gamma} \mathbf{q}^{n+1} + \mathbf{r}^{n+1} \right) \cdot \mathbf{v} + p^{n+1} \left(\frac{1}{\gamma} \widehat{\mathbf{q}^{n+1}} + \widehat{\mathbf{r}^{n+1}} \right) \cdot \mathbf{v} \right) ds \\ - \frac{\varepsilon^2}{\Delta t} \int_K \nabla \cdot (\phi^{n+1} \mathbf{v}^{n+1}) dK + \frac{\varepsilon^2}{\Delta t} \int_{\partial K} (\widehat{\mathbf{v}^{n+1}} \cdot \mathbf{v} \phi^{n+1} + \widehat{\phi}^{n+1} \mathbf{v}^{n+1} \cdot \mathbf{v}) ds \\ + \frac{\varepsilon^2}{\Delta t} \int_K (\mathbf{v}^{n+1} \cdot \nabla \phi^n + \phi^{n+1} \nabla \cdot \mathbf{v}^n) dK - \frac{\varepsilon^2}{\Delta t} \int_{\partial K} (\widehat{\mathbf{v}^{n+1}} \cdot \mathbf{v} \phi^n + \widehat{\phi}^{n+1} \mathbf{v}^n \cdot \mathbf{v}) ds. \end{aligned} \tag{3.26}$$

For Eq. (3.20d), we choose the test function as $\Psi = \mathbf{v}^n$, and obtain

$$\int_K \mathbf{v}^{n+1} \cdot \mathbf{v}^n dK = - \int_K \phi^{n+1} \nabla \cdot \mathbf{v}^n dK + \int_{\partial K} \widehat{\phi}^{n+1} \mathbf{v}^n \cdot \mathbf{v} ds. \quad (3.27)$$

From (3.20d), we have

$$\int_K \mathbf{v}^n \cdot \Psi dK = - \int_K \phi^n \nabla \cdot \Psi dK + \int_{\partial K} \widehat{\phi}^n \Psi \cdot \mathbf{v} ds. \quad (3.28)$$

Choosing the test function $\Psi = \mathbf{v}^{n+1}$ in (3.28), implies

$$\int_K \mathbf{v}^n \cdot \mathbf{v}^{n+1} dK = - \int_K \phi^n \nabla \cdot \mathbf{v}^{n+1} dK + \int_{\partial K} \widehat{\phi}^n \mathbf{v}^{n+1} \cdot \mathbf{v} ds. \quad (3.29)$$

By substituting (3.27) and (3.29), we have

$$\begin{aligned} & \int_K (\mathbf{v}^{n+1} \cdot \nabla \phi^n + \phi^{n+1} \nabla \cdot \mathbf{v}^n) dK - \int_{\partial K} (\widehat{\mathbf{v}}^{n+1} \cdot \mathbf{v} \phi^n + \widehat{\phi}^{n+1} \mathbf{v}^n \cdot \mathbf{v}) ds \\ & \stackrel{(3.27)}{=} \int_K (\mathbf{v}^{n+1} \cdot \nabla \phi^n - \mathbf{v}^{n+1} \cdot \mathbf{v}^n) dK - \int_{\partial K} \widehat{\mathbf{v}}^{n+1} \cdot \mathbf{v} \phi^n ds \\ & = \int_K (\mathbf{v}^{n+1} \cdot \nabla \phi^n - \mathbf{v}^{n+1} \cdot \mathbf{v}^n - \phi^n \nabla \cdot \mathbf{v}^{n+1} + \phi^n \nabla \cdot \mathbf{v}^{n+1}) dK - \int_{\partial K} \widehat{\mathbf{v}}^{n+1} \cdot \mathbf{v} \phi^n ds \\ & \stackrel{(3.29)}{=} \int_K (\mathbf{v}^{n+1} \cdot \nabla \phi^n + \phi^n \nabla \cdot \mathbf{v}^{n+1}) dK - \int_{\partial K} (\widehat{\mathbf{v}}^{n+1} \cdot \mathbf{v} \phi^n + \widehat{\phi}^n \mathbf{v}^{n+1} \cdot \mathbf{v}) ds. \end{aligned} \quad (3.30)$$

Finally, summing up Eqs. (3.26) and (3.30) over K and noticing the fluxes in (3.22)–(3.23) are from the opposite sides of ∂K as well as the boundary conditions (3.24)–(3.25), we get

$$\varepsilon^2 \int_{\Omega} \mathbf{v}^{n+1} \cdot \delta_t \mathbf{v}^{n+1} d\mathbf{x} + \int_{\Omega} ((\phi^{n+1})^3 - \phi^n) \delta_t \phi^{n+1} d\mathbf{x} + \int_{\Omega} \left(|\mathbf{w}^{n+1}|^2 + \frac{1}{\gamma} |\mathbf{q}^{n+1} + \gamma \phi^n \mathbf{w}^{n+1}|^2 \right) d\mathbf{x} = 0.$$

Then

$$\begin{aligned} & \varepsilon^2 \int_{\Omega} \mathbf{v}^{n+1} \cdot \delta_t \mathbf{v}^{n+1} d\mathbf{x} + \frac{1}{\Delta t} \int_{\Omega} \left(\frac{1}{4} (\phi^{n+1})^4 - \frac{1}{2} (\phi^{n+1})^2 \right) d\mathbf{x} - \frac{1}{\Delta t} \int_{\Omega} \left(\frac{1}{4} (\phi^n)^4 - \frac{1}{2} (\phi^n)^2 \right) d\mathbf{x} \\ & + \frac{1}{4\Delta t} \int_{\Omega} ((2 + 2(\phi^{n+1})^2 + (\phi^n + \phi^{n+1})^2) (-\phi^{n+1} + \phi^n)^2) d\mathbf{x} \\ & + \int_{\Omega} \left(|\mathbf{w}^{n+1}|^2 + \frac{1}{\gamma} |\mathbf{q}^{n+1} + \gamma \phi^n \mathbf{w}^{n+1}|^2 \right) d\mathbf{x} = 0, \end{aligned}$$

therefore we obtain the discrete energy stability

$$\int_{\Omega} \left(\frac{1}{4} (\phi^{n+1})^4 - \frac{1}{2} (\phi^{n+1})^2 + \frac{\varepsilon^2}{2} |\mathbf{v}^{n+1}|^2 \right) d\mathbf{x} \leq \int_{\Omega} \left(\frac{1}{4} (\phi^n)^4 - \frac{1}{2} (\phi^n)^2 + \frac{\varepsilon^2}{2} |\mathbf{v}^n|^2 \right) d\mathbf{x}. \quad \square$$

Remark 3.1. The unconditional energy stability is proved. But as for the solvability of the convex splitting scheme, the proof is not easy in the LDG framework. Even though the auxiliary variables in the LDG method give the easy treatment for nonlinear and high order derivative terms, the theoretical analysis of solvability for the LDG is more troublesome because of the auxiliary variables. We will leave it to our future work.

3.3. Algorithm flowchart and the multigrid solver

Given ϕ^n , μ^n and p^n , the algorithm to get ϕ^{n+1} , μ^{n+1} and p^{n+1} is

1. We choose a local basis in cell K , then \mathbf{w}^{n+1} , \mathbf{v}^{n+1} , \mathbf{s}^{n+1} , \mathbf{q}^{n+1} and r^{n+1} can be eliminated from Eqs. (3.20b), (3.20d), (3.20e), (3.21b) and (3.21c), respectively, by simply inverting a small mass matrix in each case.

Table 4.1

Accuracy test for [Example 4.1](#) at $t = 0.5$. To maintain the accuracy, the time steps are chosen as $\Delta t = 0.1\Delta x$, $\Delta t = 0.4\Delta x^2$ and $\Delta t = 0.4\Delta x^3$ for \mathcal{P}^0 , \mathcal{P}^1 and \mathcal{P}^2 approximation, respectively. $\varepsilon = 0.2$, $\gamma = 2.0$.

| | N | L^2 error | Order | L^∞ error | Order |
|-----------------|-----|-------------|-------|------------------|-------|
| \mathcal{P}^0 | 16 | 3.66E-01 | – | 1.73E-01 | – |
| | 32 | 1.69E-01 | 1.11 | 7.92E-02 | 1.13 |
| | 64 | 8.32E-02 | 1.02 | 4.23E-02 | 0.91 |
| | 128 | 4.17E-02 | 0.99 | 2.18E-02 | 0.95 |
| \mathcal{P}^1 | 16 | 1.59E-01 | – | 4.59E-02 | – |
| | 32 | 4.86E-02 | 1.71 | 1.47E-02 | 1.64 |
| | 64 | 1.32E-02 | 1.88 | 4.14E-03 | 1.83 |
| | 128 | 3.38E-03 | 1.96 | 1.07E-03 | 1.95 |
| \mathcal{P}^2 | 16 | 7.14E-02 | – | 1.96E-02 | – |
| | 32 | 1.04E-02 | 2.77 | 3.12E-03 | 2.66 |
| | 64 | 1.33E-03 | 2.97 | 3.97E-04 | 2.96 |
| | 128 | 1.64E-04 | 3.02 | 4.90E-05 | 3.02 |

2. We get a system of three coupled second-order nonlinear equations for $\{\phi^{n+1}, \mu^{n+1}, p^{n+1}\}$

$$\begin{cases} \phi^{n+1} = L_1(\mu^{n+1}, p^{n+1}, \phi^n), \\ \mu^{n+1} = L_2(\phi^{n+1}, \phi^n), \\ p^{n+1} = L_3(\mu^{n+1}, \phi^n). \end{cases} \tag{3.31}$$

3. We solve the system of nonlinear equations (3.31) at each time step and get ϕ^{n+1} , μ^{n+1} and p^{n+1} .

The semi-implicit convex splitting scheme (3.19) is stable regardless of time step size. However, we need to solve a system of nonlinear algebraic equations at each time step. The overall performance highly depends on the performance of the solver. Traditionally iterative solution methods such as Gauss–Seidel method and Newton method suffer from slow convergence rates.

We apply the nonlinear FAS multigrid method to solve the nonlinear equations and we will numerically show the nearly optimal convergence of the multigrid solver in the next section. For detailed descriptions of the FAS multigrid algorithm and the Gauss–Seidel smoother, we refer the readers to [Appendix A](#) and [Appendix B](#), respectively.

4. Numerical tests

In this section, we perform numerical experiments of the LDG method applied to the Cahn–Hilliard–Hele–Shaw system. We consider the convex splitting scheme (3.19) and the resulting nonlinear equations are solved by the FAS multigrid method. For the spatial discretization, we use uniform meshes. All the computations are performed in double precision.

Example 4.1 (Convergence of the multigrid solver). To demonstrate the superiority of the multigrid solver, we present the convergence rates of the method. For the tests we take the exact solution of

$$\phi(x, y, t) = e^{-2t} \sin(x) \sin(y), \tag{4.32}$$

with the source term $f(x, y, t)$, where $f(x, y, t)$ is a given function so that make the exact solution. The initial condition is

$$\phi(x, y, 0) = \sin(x) \sin(y), \tag{4.33}$$

and the domain is $[0, 2\pi] \times [0, 2\pi]$ with periodic boundary conditions. The time step is fixed as $\Delta t = 0.01\Delta x$ and the spatial step size varies from $\Delta x = 2\pi/32$ to $\Delta x = 2\pi/128$ in the test results.

We present the convergence rates of the multigrid solver at the 10th time step for various choices of ε and γ in [Fig. 4.1](#). From [Fig. 4.1](#), we can see the optimal convergence of the multigrid solver for \mathcal{P}^1 approximation and nearly optimal convergence for \mathcal{P}^2 approximation, with $\varepsilon = 0.1$ and $\varepsilon = 0.2$. When ε is smaller ($\varepsilon = 0.05$), the nearly optimal convergence for \mathcal{P}^1 and \mathcal{P}^2 approximation are shown.

The L^2 and L^∞ errors and numerical orders of accuracy at time $t = 0.5$ are contained in [Table 4.1](#). To maintain the accuracy, the time steps are chosen as $\Delta t = 0.1\Delta x$, $\Delta t = 0.4\Delta x^2$ and $\Delta t = 0.4\Delta x^3$ for \mathcal{P}^0 , \mathcal{P}^1 and \mathcal{P}^2 approximation, respectively. We can see that the method with \mathcal{P}^k elements gives $(k + 1)$ th order of accuracy in both L^2 and L^∞ norms. What we should keep in mind is that the choice of this refinement path has nothing to do with any time step restriction for stability.

Example 4.2 (Spinodal decomposition and energy dissipation). We consider the convex splitting scheme (3.19) with the LDG spatial discretization. The initial data is a random field of values that are uniformly distributed about the average composition $\bar{\phi} = -0.05$, with amplitude 0.05. The domain is $[0, 6.4] \times [0, 6.4]$ and the boundary conditions are (2.4). We take $\epsilon = 0.03$. For γ we use the values 0.0 and 4.0.

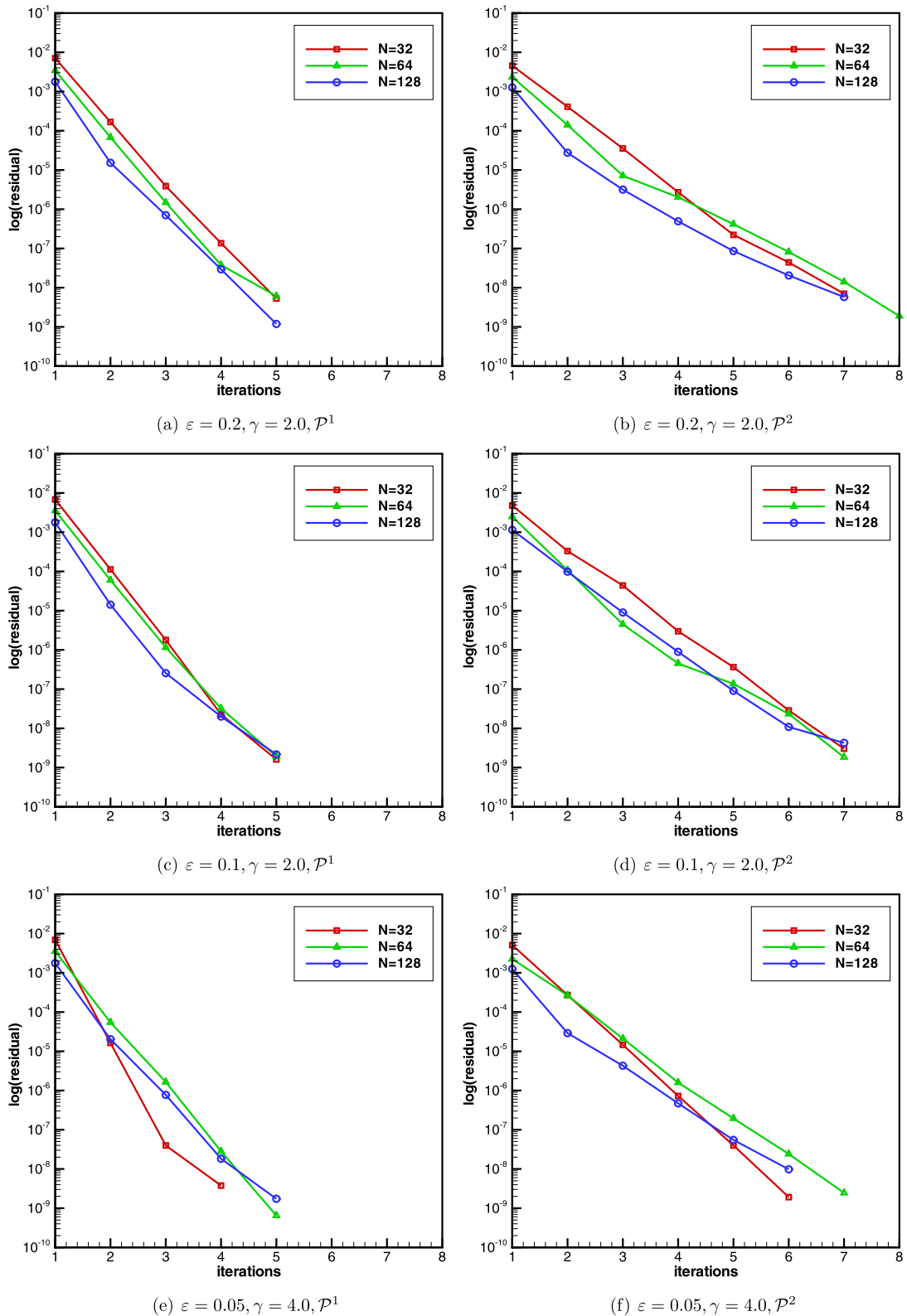


Fig. 4.1. Convergence rates of multigrid solver with \mathcal{P}^1 and \mathcal{P}^2 approximation for various choices of ε and γ .

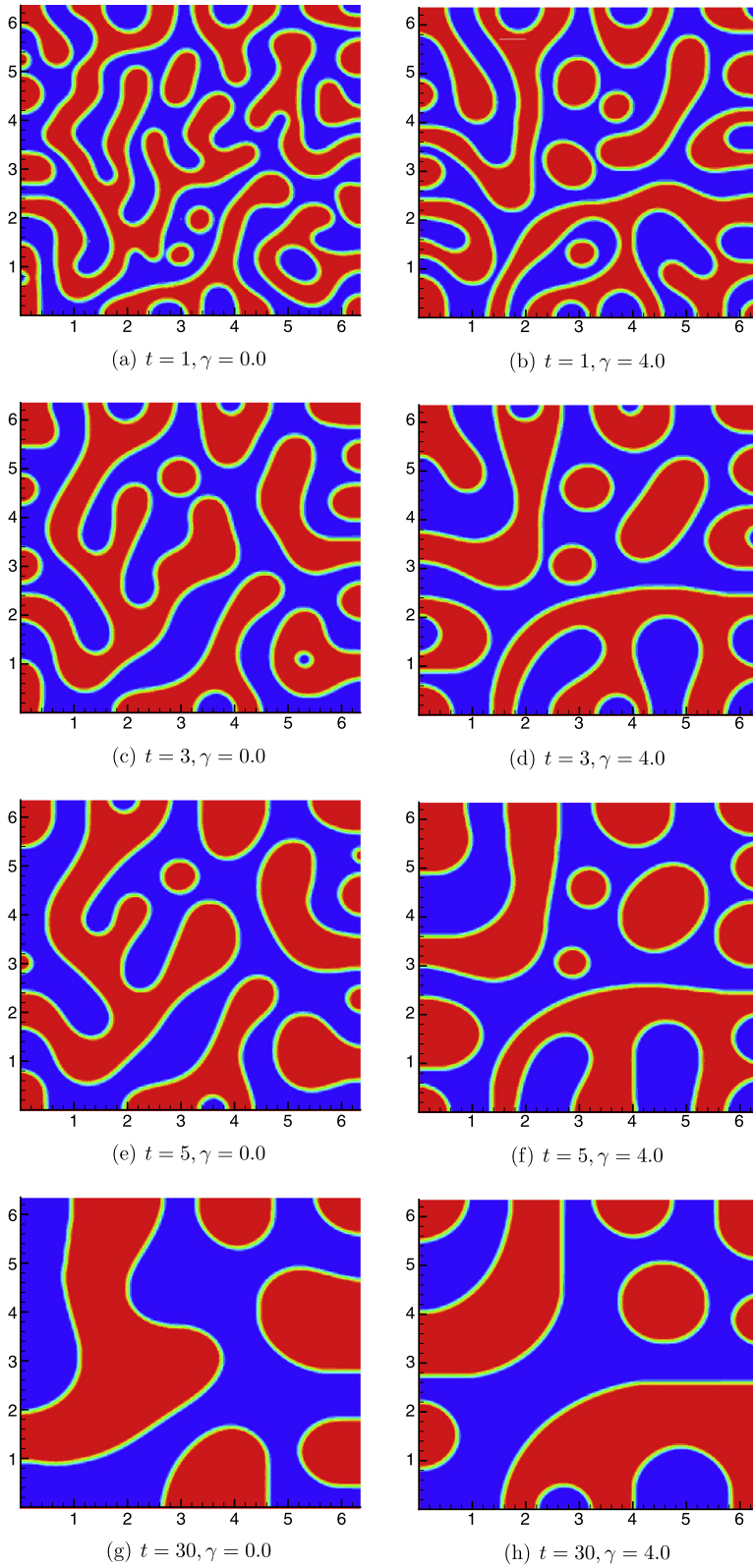


Fig. 4.2. The time evolution of the CHHS system implemented with scheme (3.19) for Example 4.2.

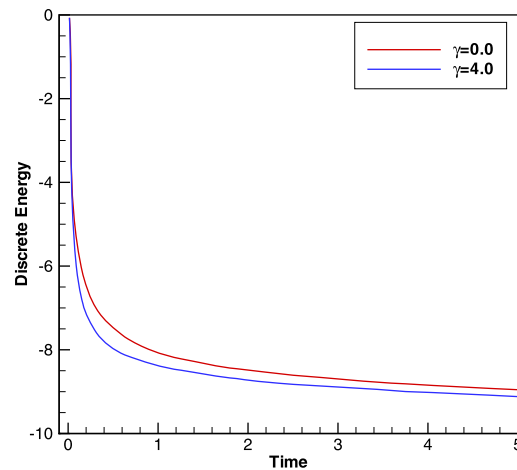


Fig. 4.3. Energy trace of numerical solution for Example 4.2.

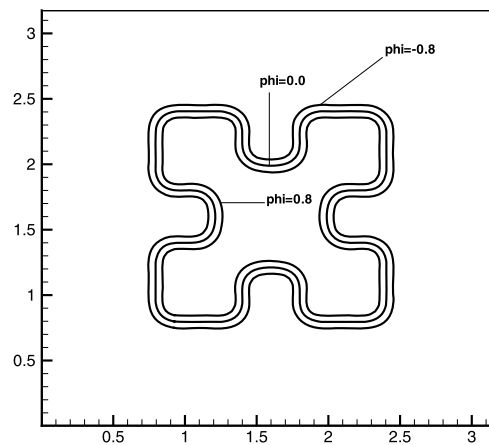


Fig. 4.4. The initial shape for Example 4.3. The contours $\phi = -0.8, 0.0$ and 0.8 are shown.

Fig. 4.2 shows the simulations with different γ at the times $t = 1.0, 3.0, 5.0$ and 30.0 . From Fig. 4.2, we can see that identified particles have a smaller shaper factor for $\gamma = 4.0$ than for $\gamma = 0.0$ when compared at the same time. In spinodal decomposition, particles can coarsen, i.e. large particles may grow at the expense of smaller particles. Fig. 4.2 shows statistically similar patterns in the numerical solution as those in Wise [22].

The energy trace with different γ is presented in Fig. 4.3. We can see that the discrete energy is non-increasing in time, which agrees with the theoretical result. In the early stages of decomposition, the energy is closely matched. Then in the latter stages of decomposition, the energy decrease faster for larger γ .

Example 4.3 (*Shape relaxation and energy dissipation*). We consider the convex splitting scheme (3.19). The initial shape is shown in Fig. 4.4. The domain is $[0, 3.2] \times [0, 3.2]$ and the boundary conditions are (2.4). We take $\epsilon = 0.03$. Three different values for γ , namely, $0.0, 2.0$ and 10.0 are used. The results of the simulations at different times are presented in Fig. 4.5. We can see that with the initial shape 4.4, the isolated shapes will relax to a circular disk. For larger γ , the shapes relax faster to a circular disk. What we should notice in Fig. 4.5 is that the interfacial thickness—which can, roughly speaking, be measured as the distance between the contours $\phi = -0.8$ and $\phi = 0.8$ appears to be invariant with respect to different γ . The energy trace with different γ is presented in Fig. 4.6. We can see that the discrete energy is non-increasing in time, which agrees with the theoretical result. The energy decrease faster for larger γ . The numerical results compare very well with the numerical calculations performed by Wise [22].

We consider the scheme (3.19) with the square initial shape presented in Fig. 4.7. The results of the simulations at different times are presented in Fig. 4.8. For the initial shape of a triangle as is shown in Fig. 4.9, the simulations at different times are presented in Fig. 4.10. In all cases the shape relaxes to a disk. We also can see that larger positive values of γ will lead to an increase in the speed with which shapes relax.

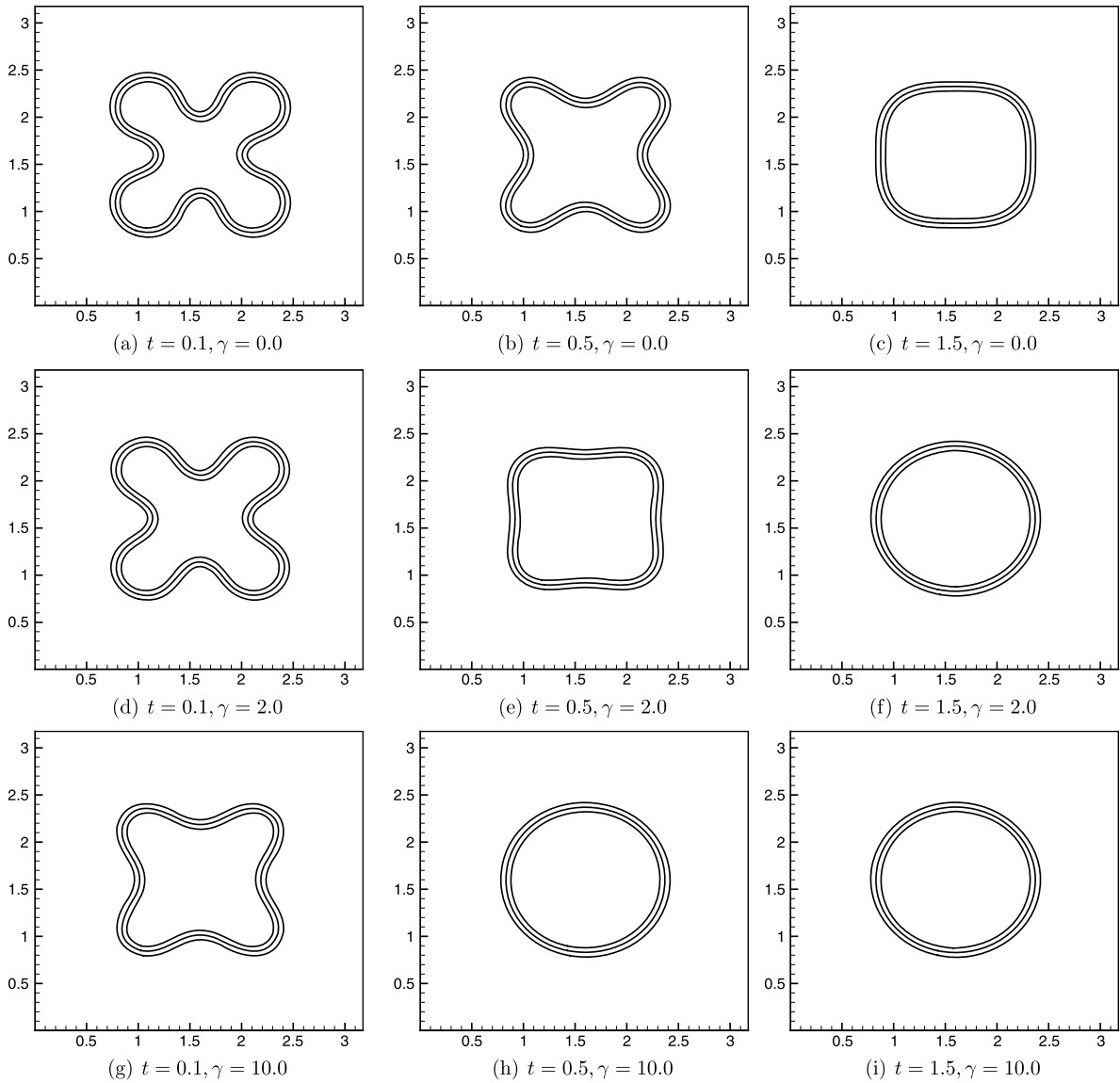


Fig. 4.5. The results of CHHS system implemented with scheme (3.19) with the respectively values $\gamma = 0.0, 2.0$ and 10.0 . The initial shape is shown in Fig. 4.4. We show the contours $\phi = -0.8, 0.0$ and 0.8 .

Finally, we remark that the numerical results presented above are qualitatively very similar to those presented in [22]. But, what we should have in mind is that the DG spatial discretization does allow for more flexibility than that of the finite difference method in several other ways. DG methods are a class of finite element methods, which can handle the irregular computational domain and complex boundary conditions easily comparing with the finite difference methods. Meanwhile, since the basis functions can be completely discontinuous, discontinuous Galerkin methods have the flexibility which is not shared by typical finite element methods, such as the allowance of arbitrary triangulation with hanging nodes, complete freedom in changing the polynomial degrees in each element independent of that in the neighbors (*p*-adaptivity), and extremely local data structure (elements only communicate with immediate neighbors regardless of the order of accuracy of the scheme) and the resulting embarrassingly high parallel efficiency.

5. Conclusion

In this paper, we have constructed a fully-discrete LDG method for the Cahn–Hilliard–Hele–Shaw system. The energy stability is proved for the semi-discrete scheme firstly. As for the time discretization, we presented a convex splitting semi-implicit scheme and proved the unconditional energy stability. That is, the energy is always non-increasing in time regardless of time step sizes. The use of the semi-implicit method will result in a nonlinear system of algebraic equations

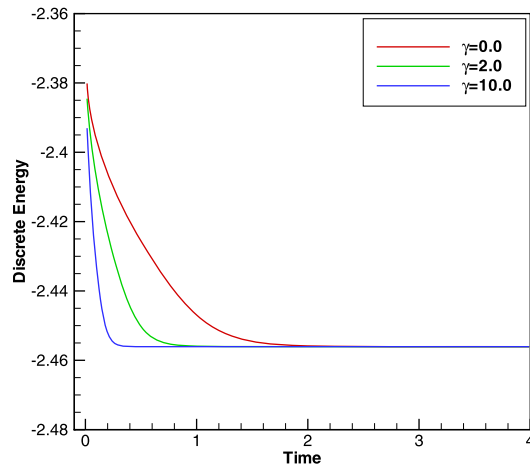


Fig. 4.6. Energy trace of numerical solution for Example 4.3 with the initial shape 4.4.

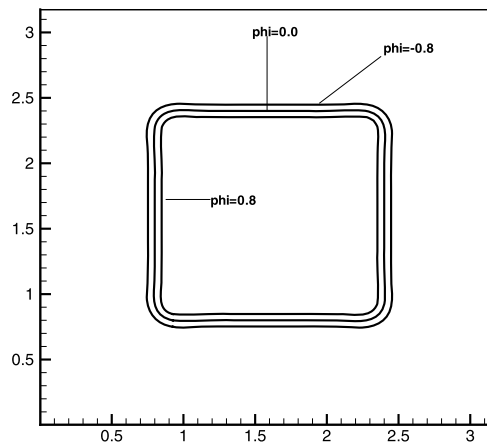


Fig. 4.7. The square initial shape for Example 4.3. The contours $\phi = -0.8, 0.0$ and 0.8 are shown.

at each time step and the FAS multigrid solver is adopted to solve the system. We show numerically that the number of the multigrid iterations is nearly independent of the problem size and is of nearly optimal complexity. Although not addressed in this paper, the local discontinuous Galerkin methods are flexible for general geometry, unstructured meshes and h - p adaptivity, and have excellent parallel efficiency.

In future, the high order schemes in time and the theoretical analysis for the LDG scheme, such as solvability and error estimates etc., will be our further research topics.

Appendix A. The nonlinear FAS multigrid solver

We start by introducing the basic notations to describe the general setting of a two-level method. Together with the family of partitions $\{\mathcal{T}_h\}_{h>0}$ used for the LDG discretization, we consider a coarse family of mesh partitions, $\{\mathcal{T}_H\}_{H>0}$ with $H > h$ and satisfying the basic assumption $\mathcal{T}_H \subset \mathcal{T}_h$. One can think $H = 2h$, since in many circumstances it will already be coarse enough. Associated to the coarse mesh partition we have the corresponding finite element space V_H which is defined as

$$V_H = \{\varphi: \varphi|_D \in \mathcal{P}^k(D), \forall D \in \mathcal{T}_H\}. \quad (1.34)$$

To link functions in both spaces, we define the prolongation and restriction operators. The prolongation operator $P_{hH}: V_h \rightarrow V_H$ is defined as the natural inclusion. The restriction operator $R_{Hh}: V_H \rightarrow V_h$ is defined as the transpose of P_{hH} with respect to the standard L^2 -inner product. That is, it is obtained by solving:

$$\sum_{D \in \mathcal{T}_H} \int_D R_{Hh}(u_h) v_H dx = \sum_{D \in \mathcal{T}_h} \int_D u_h P_{hH}(v_H), dx, \quad \forall v_H \in V_H. \quad (1.35)$$

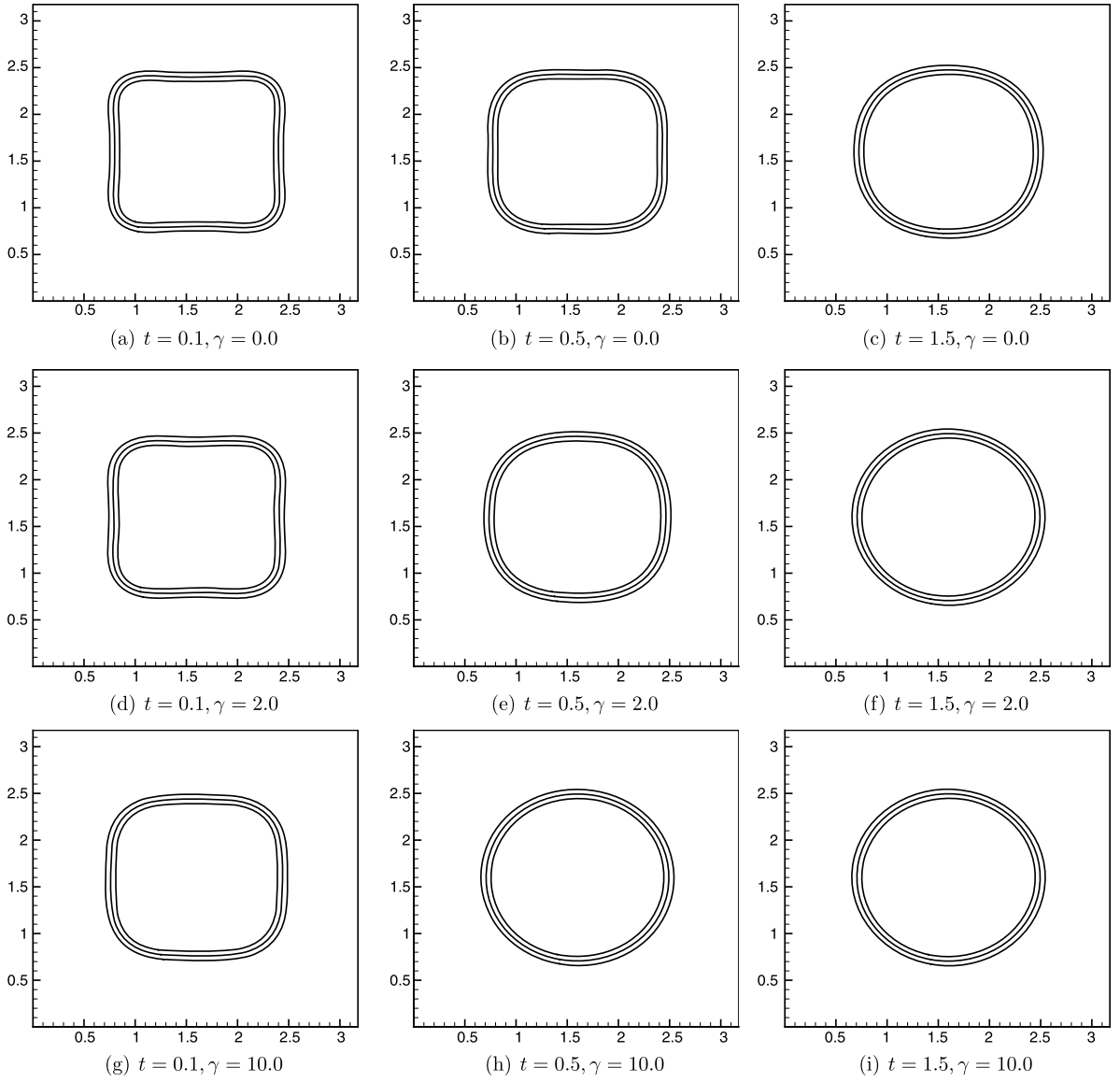


Fig. 4.8. The results of CHHS system implemented with scheme (3.19) with the respectively values $\gamma = 0.0, 2.0$ and 10.0 . The initial shape is shown in Fig. 4.7. We show the contours $\phi = -0.8, 0.0$ and 0.8 .

The nonlinear scheme (3.19) requires the solution at each time step of an algebraic nonlinear system, i.e.

$$N_h(u_h) = f_h, \tag{1.36}$$

and the nonlinear FAS multigrid method is introduced to solve the system. Following [21], we illustrate the FAS bi-grid cycle as follows:

Algorithm 1: Two-grid cycle. Starting with an initial approximation, say u_h^m :

1. **Pre-relaxation:** apply ν_1 pre-relaxation sweeps to (1.36) with u_h^m the initial approximation and obtain \bar{u}_h^m .
2. **Coarse-grid correction:** compute the coarse level initial iterate

$$\bar{u}_H^m = R_{Hh}\bar{u}_h^m, \tag{1.37}$$

update the solution \bar{u}_h^m by a coarse-grid correction step, solve the problem on coarse grid

$$N_H(v_H) = N_H(\bar{u}_H^m) + R_{Hh}(f_h - N_h(\bar{u}_h^m)) \tag{1.38}$$

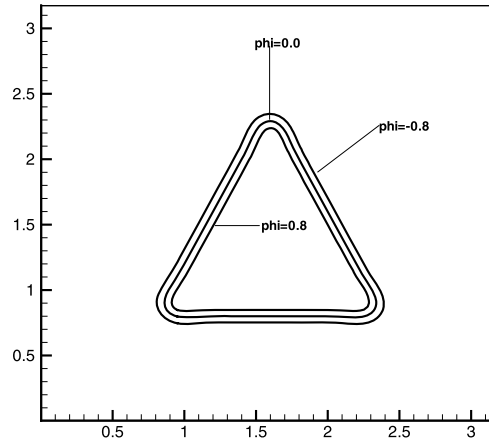


Fig. 4.9. The triangle initial shape for Example 4.3. The contours $\phi = -0.8, 0.0$ and 0.8 are shown.

and set $u_h^{CG} = \bar{u}_h^m + P_{hH}(v_H - \bar{u}_H^m)$.

3. **Post-relaxation:** start with u_h^{CG} , apply v_2 post-relaxation sweeps to (1.36) and obtain u_h^{m+1} .

Solving the coarse grid problem at the second step of the above algorithm could be done again with the two-level algorithm. Hence, the nonlinear FAS multigrid algorithm is defined by applying the two-level algorithm recursively.

Appendix B. The Gauss–Seidel smoother

In this subsection, we give a detailed discussion of the smoothing operator for our problem. Firstly, we look at the implementation of the LDG scheme (3.20)–(3.21). If a local basis of $\mathcal{P}^k(K)$ is chosen and denoted as $\phi_{i,j}^l(x, y)$ for $l = 1, 2, \dots, L = (k + 1)(k + 2)/2$, we can express the numerical solution $\phi^{n+1}(x, y)$ as

$$\phi^{n+1}(x, y) = \sum_{l=1}^L \phi_{i,j}^l \phi_{i,j}^l(x, y),$$

and we should solve for the coefficients $\phi_{i,j}^{n+1} = [\phi_{i,j}^1, \dots, \phi_{i,j}^L]^T$. Then, we consider the equation

$$\int_K \frac{\phi^{n+1} - \phi^n}{\Delta t} \varphi dK = - \int_K (\mathbf{w}^{n+1} + \mathbf{s}^{n+1}) \cdot \nabla \varphi dK + \int_{\partial K} (\widehat{\mathbf{w}^{n+1}} \cdot \mathbf{v} + \widehat{\mathbf{s}^{n+1}} \cdot \mathbf{v}) \varphi ds,$$

where $\mathbf{w}^{n+1} = [w_1^{n+1}, w_2^{n+1}]^T$, $\mathbf{s} = [s_1^{n+1}, s_2^{n+1}]^T$, choose $\varphi = \phi_{i,j}^l(x, y)$, $l = 1, 2, \dots, L = (k + 1)(k + 2)/2$ and with the chosen flux for \mathbf{w}^{n+1} , \mathbf{s}^{n+1} , we have

$$\begin{aligned} \phi_{i,j}^{n+1} = & \phi_{i,j}^n + \Delta t (A(w_{1i,j}^{n+1} + s_{1i,j}^{n+1}) + B(w_{1i-1,j}^{n+1} + s_{1i-1,j}^{n+1}) \\ & + C(w_{2i,j}^{n+1} + s_{2i,j}^{n+1}) + D(w_{2i,j-1}^{n+1} + s_{2i,j-1}^{n+1})), \end{aligned}$$

where A, B, C, D are $L \times L$ matrices. Other equations in (3.20)–(3.21) can be discreted similarly. Then, by the algorithm shown in Section 3.3, we can eliminate some auxiliary variables and get a system of three coupled second-order nonlinear equations for $\{\phi_{i,j}^{n+1}, \mu_{i,j}^{n+1}, p_{i,j}^{n+1}\}$.

For smoothing, we use a nonlinear Gauss–Seidel method. Let m be the index for the lexicographic Gauss–Seidel. And the Gauss–Seidel smoothing is as follows: for every (i, j) , stepping lexicographically from $(1, 1)$ to (N, N) , find $\phi_{i,j}^{m+1}$, $\mu_{i,j}^{m+1}$ and $p_{i,j}^{m+1}$ that solve

$$\begin{aligned} \phi_{i,j}^{m+1} - \Delta t XY \mu_{i,j}^{m+1} - \Delta t XY_1 p_{i,j}^{m+1} = & \phi_{i,j}^n + \Delta t (XM \mu_{i-1,j}^{m+1} + XP \mu_{i+1,j}^m + YM \mu_{i,j-1}^{m+1} + YP \mu_{i,j+1}^m) \\ & + \Delta t (XM_1 p_{i-1,j}^{m+1} + XP_1 p_{i+1,j}^m + YM_1 p_{i,j-1}^{m+1} + YP_1 p_{i,j+1}^m), \end{aligned} \tag{2.39}$$

$$\begin{aligned} -Jac^m \phi_{i,j}^{m+1} + \mu_{i,j}^{m+1} + \varepsilon^2 XY_2 \phi_{i,j}^{m+1} = & -\phi_{i,j}^n + r_{i,j}^m - Jac^m \phi_{i,j}^m \\ & - \varepsilon^2 (XM_2 \phi_{i-1,j}^{m+1} + XP_2 \phi_{i+1,j}^m + YM_2 \phi_{i,j-1}^{m+1} + YP_2 \phi_{i,j+1}^m) \end{aligned} \tag{2.40}$$

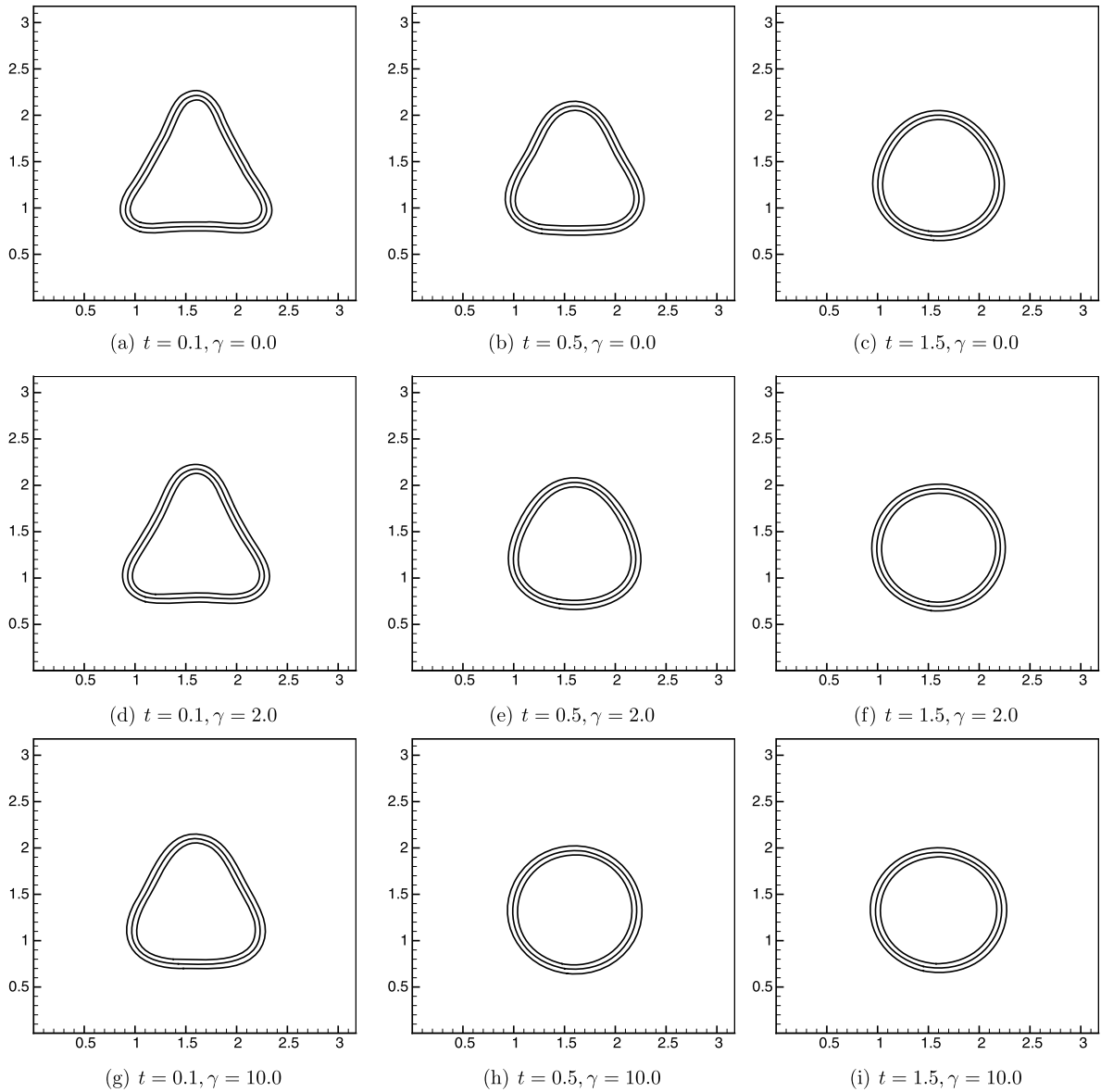


Fig. 4.10. The results of CHHS system implemented with scheme (3.19) with the respectively values $\gamma = 0.0, 2.0$ and 10.0 . The initial shape is shown in Fig. 4.9. We show the contours $\phi = -0.8, 0.0$ and 0.8 .

$$\begin{aligned}
 -XY_2 p_{i,j}^{m+1} - \gamma XY_1 \mu_{i,j}^{m+1} &= XM_2 p_{i-1,j}^{m+1} + XP_2 p_{i+1,j}^m + YM_2 p_{i,j-1}^{m+1} + YP_2 p_{i,j+1}^m \\
 &\quad + \gamma (XM_1 \mu_{i-1,j}^{m+1} + XP_1 \mu_{i+1,j}^m + YM_1 \mu_{i,j-1}^{m+1} + YP_1 \mu_{i,j+1}^m),
 \end{aligned}
 \tag{2.41}$$

where $XM, XM_1, XM_2, XP, XP_1, XP_2, YM, YM_1, YM_2, YP, YP_1, YP_2, XY, XY_1, XY_2$ are $L \times L$ matrices. Note that we have linearized the cubic term using a local Newton approximation. Let $r^m = (\phi^m)^3$, we have

$$\int_{I_{i,j}} r^m \phi_{i,j}^l(x, y) dx dy = \int_{I_{i,j}} (\phi^m)^3 \phi_{i,j}^l(x, y) dx dy, \quad l = 1, \dots, L$$

then we can get $r_{i,j}^m$. And Jac^m is a Jacobian matrix, i.e.

$$\frac{\partial (r_{i,j}^{1m}, \dots, r_{i,j}^{Lm})}{\partial (\phi_{i,j}^{1m}, \dots, \phi_{i,j}^{Lm})}.$$

The $3L \times 3L$ linear system defined by (2.39)–(2.41) can be solved by Cramer’s Rule and thus we get $\phi_{i,j}^{m+1}, \mu_{i,j}^{m+1}$ and $p_{i,j}^{m+1}$.

One full block Gauss–Seidel relaxation has concluded when we have stepped lexicographically through all the grid points, from $(1, 1)$ to (N, N) .

References

- [1] J.W. Barrett, J.F. Blowey, Finite element approximation of a model for phase separation of a multi-component alloy with non-smooth free energy, *Numer. Math.* 77 (1997) 1–34.
- [2] J.W. Barrett, J.F. Blowey, H. Garcke, Finite element approximation of the Cahn–Hilliard equation with degenerate mobility, *SIAM J. Numer. Anal.* 37 (1999) 286–318.
- [3] J.W. Barrett, J.F. Blowey, H. Garcke, On fully practical finite element approximations of degenerate Cahn–Hilliard systems, *Math. Model. Numer. Anal.* 35 (2001) 713–748.
- [4] F. Bassi, S. Rebay, A high-order accurate discontinuous finite element method for the numerical solution of the compressible Navier–Stokes equations, *J. Comput. Phys.* 131 (1997) 267–279.
- [5] J.W. Cahn, On spinodal decomposition, *Acta Metall.* 9 (1961) 795–801.
- [6] B. Cockburn, C.-W. Shu, TVB Runge–Kutta local projection discontinuous Galerkin finite element method for conservation laws II: general framework, *Math. Comput.* 52 (1989) 411–435.
- [7] B. Cockburn, S.-Y. Lin, C.-W. Shu, TVB Runge–Kutta local projection discontinuous Galerkin finite element method for conservation laws III: one dimensional systems, *J. Comput. Phys.* 84 (1989) 90–113.
- [8] B. Cockburn, S. Hou, C.-W. Shu, The Runge–Kutta local projection discontinuous Galerkin finite element method for conservation laws IV: the multidimensional case, *Math. Comput.* 54 (1990) 545–581.
- [9] B. Cockburn, C.-W. Shu, The Runge–Kutta discontinuous Galerkin method for conservation laws V: multidimensional systems, *J. Comput. Phys.* 141 (1998) 199–224.
- [10] B. Cockburn, C.-W. Shu, The local discontinuous Galerkin method for time-dependent convection–diffusion systems, *SIAM J. Numer. Anal.* 35 (1998) 2440–2463.
- [11] C. Collins, J. Shen, S.M. Wise, An efficient, energy stable scheme for the Cahn–Hilliard–Brinkman system, *Commun. Comput. Phys.* 13 (2013) 929–957.
- [12] D.J. Eyre, Systems of Cahn–Hilliard equations, *SIAM J. Appl. Math.* 53 (1993) 1686–1712.
- [13] X.B. Feng, S.M. Wise, Analysis of a Darcy–Cahn–Hilliard diffuse interface model for the Hele–Shaw flow and its fully discrete finite element approximation, *SIAM J. Numer. Anal.* 50 (2012) 1320–1343.
- [14] D. Furihata, A stable and conservative finite difference scheme for the Cahn–Hilliard equation, *Numer. Math.* 87 (2001) 675–699.
- [15] R. Guo, Y. Xu, Efficient solvers of discontinuous Galerkin discretization for the Cahn–Hilliard equations, *J. Sci. Comput.* 58 (2014) 380–408, <http://dx.doi.org/10.1007/s10915-013-9738-4>.
- [16] D. Kay, R. Welford, A multigrid finite element solver for the Cahn–Hilliard equation, *J. Comput. Phys.* 212 (2006) 288–304.
- [17] J. Kim, K. Kang, J. Lowengrub, Conservative multigrid methods for Cahn–Hilliard fluids, *J. Comput. Phys.* 193 (2004) 511–543.
- [18] J. Kim, K. Kang, J. Lowengrub, Conservative multigrid methods for ternary Cahn–Hilliard systems, *Commun. Math. Sci.* 2 (2004) 53–77.
- [19] W.H. Reed, T.R. Hill, Triangular mesh method for the neutron transport equation, Technical report LA-UR-73-479, Los Alamos Scientific Laboratory, Los Alamos, NM, 1973.
- [20] Z.Z. Sun, A second-order accurate linearized difference scheme for the two-dimensional Cahn–Hilliard equation, *Math. Comput.* 64 (1995) 1463–1471.
- [21] U. Trottenberg, C. Oosterlee, A. Schüller, *Multigrid*, Academic Press, New York, 2005.
- [22] S.M. Wise, Unconditionally stable finite difference, nonlinear multigrid simulation of the Cahn–Hilliard–Hele–Shaw system of equations, *J. Sci. Comput.* 44 (2010) 38–68.
- [23] Y. Xia, Y. Xu, C.-W. Shu, Local discontinuous Galerkin methods for the Cahn–Hilliard type equations, *J. Comput. Phys.* 227 (2007) 472–491.
- [24] Y. Xia, Y. Xu, C.-W. Shu, Application of the local discontinuous Galerkin method for the Allen–Cahn/Cahn–Hilliard system, *Commun. Comput. Phys.* 5 (2009) 821–835.
- [25] Y. Xu, C.-W. Shu, Local discontinuous Galerkin methods for high-order time-dependent partial differential equations, *Commun. Comput. Phys.* 7 (2010) 1–46.
- [26] J. Yan, C.-W. Shu, A local discontinuous Galerkin method for KdV type equations, *SIAM J. Numer. Anal.* 40 (2002) 769–791.
- [27] J. Yan, C.-W. Shu, Local discontinuous Galerkin methods for partial differential equations with higher order derivatives, *J. Sci. Comput.* 17 (2002) 27–47.